4366 *Chem. Mater.* **2009,** *21,* 4366–4373
DOI:10.1021/cm900210m

CHEMISTRY OF MATERIALS
Article

Synthesis of Mn-Substituted Titania Nanosheets and Ferromagnetic Thin Films with Controlled Doping

Xiaoping Dong,[†] Minoru Osada,*[,†,‡] Hidekazu Ueda,[†] Yasuo Ebina,[†,‡] Yoshinori Kotani,[§] Kanta Ono,[§] Shigenori Ueda,[⊥] Keisuke Kobayashi,[⊥] Kazunori Takada,[†,‡] and Takayoshi Sasaki[†,‡]

[†]*International Center for Materials Nanoarchitectonics, National Institute for Materials Science, Tsukuba, Ibaraki 305-0044, Japan,* [‡]*CREST, Japan Science and Technology Agency, Kawaguchi, Saitama 332-0012, Japan,* [§]*Institute of Materials Structure Science, High Energy Accelerator Research Organization, Tsukuba, Ibaraki 305-0801, Japan, and* [⊥]*NIMS Beamline Station at SPring-8, National Institute for Materials Science, Hyogo 679-5148, Japan*

Received January 23, 2009. Revised Manuscript Received July 24, 2009

We report the synthesis of Mn-substituted titania nanosheets and the preparation of room-temperature ferromagnetic thin films via layer-by-layer assembly of these nanosheets. $Ti_{(5.2-2x)/6}Mn_{x/2}O_2$ ($x = 0.0-0.4$) nanosheets were synthesized by delaminating layered titanates [$K_{0.8}Ti_{(5.2-2x)/3}Li_{(0.8-x)/3}Mn_xO_4$], in which the Mn content was systematically controlled by Li^+ doping. We found that Mn content in the host layers was preserved upon exfoliation, and controlled Mn doping was achieved in exfoliated $Ti_{(5.2-2x)/6}Mn_{x/2}O_2$ ($x = 0.0-0.4$) nanosheets, where Li^+ ions were completely extracted by acid-exchange reaction in the exfoliation process. The multilayer films of $Ti_{(5.2-2x)/6}Mn_{x/2}O_2$ ($x = 0.0-0.4$) nanosheets exhibit a clear magnetic hysteresis loop at room-temperature in similar to what observed in ferromagnetic $Ti_{1-x}Co_xO_2$ nanosheets. Electronic absorption, magnetic circular dichroism, and hard X-ray photoelectron spectroscopy were used to identify Mn-derived states, and analyze the properties of these states related to ferromagnetism. The first-principles calculation of $Ti_{(5.2-2x)/6}Mn_{x/2}O_2$ was also employed to characterize the doping effect on electronic structures.

Introduction

The recent thrust in the search for potential spintronic materials has generated a concerted effort among researchers to synthesize and explore diluted magnetic semiconductors (DMS).[1] An area of current interest is the search for high-T_C ferromagnetism in DMS oxides for beneficial use in practical spintronic devices. Room-temperature (RT) ferromagnetism is reported for some 3d transition-metal-doped TiO_2, ZnO, or SnO_2 thin films[2−4] synthesized by vacuum deposition methods such as laser ablation and molecular beam epitaxy, but several studies also report the absence of ferromagnetism in similar films. This class of materials appears to be extremely sensitive to the conditions of sample preparation and postannealing treatment, and the ultimate source of observed ferromagnetism remains unresolved. In particular, the occurrence of undesirable impurity phases due to clustering and phase segregation of magnetic dopants has plagued efforts at materials development with the origin of ferromagnetism in DMS materials.[5] Understanding and controlling ferromagnetic ordering in DMS thus remains a significant challenge.

The difficulties in controlling the chemical properties of DMS synthesized by vacuum deposition have motivated us to investigate direct chemical methods for the synthesis of DMS. Direct synthetic methods might allow better control over chemical composition and dopant speciation compared to vacuum deposition methods, and might subsequently provide a better experimental basis for understanding and ultimately controlling the magnetic properties of this class of materials. Furthermore, a direct chemical approach might allow the preparation of DMS in unprecedented forms. Recent progress in chemical synthesis of DMS quantum dots, nanorods and nanowires such as TiO_2:Co, ZnO:Mn indicates that these

*Corresponding author. E-mail: osada.minoru@nims.go.jp.

(1) (a) Ohno, H. *Science* **1998**, *281*, 951. (b) Wolf, S. A.; Awschalom, D. D.; Buhrman, R. A.; Daughton, J. M.; Von Molnár, S.; Roukes, M. L.; Chtchelkanova, A. Y.; Treger, D. M. *Science* **2001**, *294*, 1488. (c) Berciu, M.; Bhatt, R. N. *Phys. Rev. Lett.* **2001**, *87*, 107203.
(2) (a) Matsumoto, Y.; Murakami, M.; Shono, T.; Hasegawa, T.; Fukumura, T.; Kawasaki, M.; Ahmet, P.; Chikyow, T.; Koshihara, S.; Koinuma, H. *Science* **2001**, *291*, 854. (b) Park, W. K.; Ortega-Hertogs, R. J.; Moodera, J. S.; Punnoose, A.; Seehra, M. S. *J. Appl. Phys.* **2002**, *91*, 8093.
(3) (a) Sharma, P.; Gupta, A.; Rao, K. V.; Owens, F. J.; Sharma, R.; Ahuja, R.; Guillen, J. M. O.; Johansson, B.; Gehring, G. A. *Nat. Mater.* **2003**, *2*, 673. (b) Cho, Y. M.; Choo, W. K.; Kim, H.; Kim, D.; Ihm, Y. *Appl. Phys. Lett.* **2002**, *80*, 3358.
(4) (a) Fitzgerald, C. B.; Venkatesan, M.; Douvalis, A. P.; Huber, S.; Coey, J. M. D.; Bakas, T. *J. Appl. Phys.* **2004**, *95*, 7390. (b) Coey, J. M. D.; Douvalis, A. P.; Fitzgerald, C. B.; Venkatesan, M. *Appl. Phys. Lett.* **2004**, *84*, 1332. (c) Ogale, S. B.; Choudhary, R. J.; Buban, J. P.; Lofland, S. E.; Shinde, S. R.; Kale, S. N.; Kulkarni, V. N.; Higgins, J.; Lanci, C.; Simpson, J. R.; Browning, N. D.; Das Sarma, S.; Drew, H. D.; Greene, R. L.; Venkatesan, T. *Phys. Rev. Lett.* **2003**, *91*, 077205.
(5) (a) Kim, Y. J.; Thevuthasan, S.; Droubay, T.; Lea, A. S.; Wang, C. M.; Shutthanandan, V.; Chambers, S. A.; Sears, R. P.; Taylor, B.; Sinkovic, B. *Appl. Phys. Lett.* **2004**, *84*, 3531. (b) Stampe, P. A.; Kennedy, R. J.; Xin, Y.; Parker, J. S. *J. Appl. Phys.* **2002**, *92*, 7114.

 Published on Web 08/31/2009

routes hold promise for achieving low-dimensional DMS nanostructures.[6−8] Besides being pivotal architectural elements in magneto-optic and magneto-electronic devices, these DMS nanostructures can also be ideal model systems for studying the role of dimensionality and size effect on magnetic ordering and anisotropy. However, spin effects in DMS nanostructures are largely unexplored, and essential advances in this field would be facilitated by the development of simple methods for preparing high-quality DMS nanostructures.

We recently reported a new 2D ferromagnet based on $Ti_{1-x}M_xO_2$ (M = Fe, Co) nanosheet, a nanosized titanium oxide derived from layered titanate by exfoliation.[9,10] Compared with Co-doped TiO_2 and other bulk oxides,[2−4] $Ti_{1-x}Co_xO_2$ nanosheets have some unique features: (i) Because of the charge-neutrality requirement in the starting material ($K_{0.8}Ti_{1.6}Co_{0.4}O_4$), they are intrinsically heavily doped with a well-defined composition $[Ti_{0.8}Co_{0.2}O_2]^{0.4-}$, in which Co^{2+} ions are fully incorporated into Ti^{4+} sites and the oxidation state of Ti^{4+} and Co^{2+} is invariable. (ii) Despite a heavily doped 2D system in the dielectric ground, multilayer films of $Ti_{0.8}Co_{0.2}O_2$ nanosheets exhibit RT ferromagnetism with magnetic moment of 1.4 μ_B/Co. (iii) We also observed robust magnetic circular dichroism ($\sim 1 \times 10^4$ deg cm^{-1}) near the absorption edge at 280 nm. Furthermore, (Co/Fe) cosubstitution strongly enhances magneto-optical response ($\sim 10^5$ deg cm^{-1}) at 400−750 nm, which stems from the d−d transitions ($Co^{2+}-Fe^{3+}$) in titania nanosheets.[11] An important implication of these strategies is that such band engineering of the d−d transitions in titania nanosheets may have latent possibilities for developing a gigantic magneto-optical response in the short-wavelength region. In this context, controlled doping with other 3d substitution (such as V, Cr, Mn, Ni) is also of interest. Through a suitable choice of impurities, 3d substitution in individual nanosheets may gain oscillator strength in intramolecular d−d transitions, allowing unique magneto-optical effects.

In this paper, we report the chemical synthesis of Mn-substituted $Ti_{1-\delta}O_2$ nanosheets and the use of these 2D nanocrystals as building blocks for the fabrication of thin films showing RT ferromagnetism. A key feature of this new preparation is the use of (Li/Mn)-cosubstituted layered titanate [$K_{0.8}Ti_{(5.2-2x)/3}Li_{(0.8-x)/3}Mn_xO_4$] as a starting material for controlled Mn doping in exfoliated nanosheets. The parent material is $K_{0.8}Ti_{1.2}Mn_{0.8}O_4$ ($x = 0$), in which Mn^{3+} ions are fully incorporated into Ti^{4+} sites and interlayer K^+ ions are compensated for the minus charge arising from the substitution of Mn^{3+} for Ti^{4+}. In $K_{0.8}Ti_{1.2}Mn_{0.8}O_4$, however, controlled Mn^{3+} substitution has limited access because of both the charge-neutrality requirement and structural stability of lepidocrocite-type titanate. To overcome this problem, we consider the (Li/Mn)-cosubstituted system [$K_{0.8}Ti_{(5.2-2x)/3}Li_{(0.8-x)/3}Mn_xO_4$], in which both Li^+ and Mn^{3+} ions are incorporated into octahedral Ti^{4+} sites in the host layers and the Mn content can be systematically changed by the Li content while maintaining the charge-neutrality requirement. This (Li/Mn)-cosubstitution approach is also suitable for controlled Mn doping in exfoliated nanosheets, because Li ions in octahedral sites can be completely extracted by acid-exchange reaction in the exfoliation process.[12] Here, we investigated $Ti_{(5.2-2x)/6}Mn_{x/2}O_2$ ($x = 0.0-0.4$) nanosheets in order to study the influence of doping effect on magnetic and magneto-optical properties.

Experimental Section

Materials. TiO_2 (rutile form), K_2CO_3, Li_2CO_3, and Mn_2O_3 of 99.9% purity or higher were used as received from Rare Metallic, Co. for the synthesis of starting layered titanates. Other reagents were of analytical grade. Milli-Q filtered water (Millipore Co., > 18 Ω cm) was used throughout the experiments.

Mn-Substituted Layered Titanates and Their Conversion into Protonic Form. Starting layered titanates of $K_{0.8}Ti_{(5.2-2x)/3}Li_{(0.8-x)/3}Mn_xO_4$ ($x = 0.0-0.4$) were synthesized by solid-state reaction. Reagents such as TiO_2, K_2CO_3, Li_2CO_3, and Mn_2O_3 were weighed at a ratio of $K_{0.8}Ti_{(5.2-2x)/3}Li_{(0.8-x)/3}Mn_xO_4$ (x = 0.0, 0.1, 0.2, 0.3, 0.4), and intimately mixed by grinding. The mixture (10 g) was placed in a Pt crucible and reacted at 1073 K for 1 h. After being ground again, the mixture was then calcined at 1273 K for another 20 h.

The obtained polycrystalline samples were converted into protonic form by applying a previously reported procedure for nonsubstituted titanate.[12] The sample (1.0 g) was stirred in a 1.0 mol dm^{-3} HCl solution (100 cm^3) at room temperature. The acid solution was replaced daily with a fresh one by decantation. After treatment, the acid-exchanged titanates, $H_{(3.2-x)/3}Ti_{(5.2-2x)/3}Mn_xO_4 \cdot H_2O$, were collected by filtration, washed with copious amounts of pure water, and air-dried.

Delamination. Exfoliation of the protonic titanates [$H_{(3.2-x)/3}Ti_{(5.2-2x)/3}Mn_xO_4 \cdot H_2O$] was attempted by reaction with tetrabutylammonium hydroxide solution [$(C_4H_9)_4NOH$; hereafter TBAOH][13]; 0.4 g of protonic titanate was immersed in 100 cm^3 of TBAOH solution. Its concentration corresponded to a molar ratio of 1−10 with respect to exchangeable protons in the titanate. After 10 days of vigorous shaking, colloidal suspension of nanosheets (with translucent light-brown to dark brown color) was obtained.

Fabrication of Multilayer Films. Multilayer films of $Ti_{(5.2-2x)/6}Mn_{x/2}O_2$ nanosheets were fabricated by electrostatic layer-by-layer assembly technique previously described in detail.[14]

(6) Jayakumar, O. D.; Salunke, H. G.; Kadam, R. M.; Mohapatra, M.; Yaswant, G.; Kulshreshtha, S. K. *Nanotechnology* **2006**, *17*, 1278.
(7) Qiu, X. Q.; Li, L. P.; Li, G. S. *Appl. Phys. Lett.* **2006**, *88*, 114103.
(8) (a) Chang, Y. Q.; Wang, D. B.; Luo, X. H.; Xu, X. Y.; Chen, X. H.; Li, L.; Chen, C. P.; Wang, R. M.; Xu, J.; Yu, D. P. *Appl. Phys. Lett.* **2003**, *83*, 4020. (b) Lee, Y. H.; Yoo, J. M.; Park, D. H.; Kim, D. H.; Ju, B. K. *Appl. Phys. Lett.* **2005**, *86*, 033110.
(9) Osada, M.; Ebina, Y.; Takada, K.; Sasaki, T. *Adv. Mater.* **2006**, *18*, 295.
(10) Osada, M.; Ebina, Y.; Fukuda, K.; Ono, K.; Takada, K.; Yamaura, K.; Takayama-Muromachi, E.; Sasaki, T. *Phys. Rev. B* **2006**, *73*, 153301.
(11) Osada, M.; Itose, M.; Ebina, Y.; Ono, K.; Ueda, S.; Kobayashi, K.; Sasaki, T. *Appl. Phys. Lett.* **2008**, *92*, 253110.
(12) Sasaki, T.; Kooli, F.; Iida, M.; Michiue, Y.; Takenouchi, S.; Yajima, Y.; Izumi, F.; Chakoumakos, B. C.; Watanabe, M. *Chem. Mater.* **1998**, *10*, 4123.
(13) (a) Sasaki, T.; Watanabe, M.; Hashizume, H.; Yamada, H.; Nakazawa, H. *J. Am. Chem. Soc.* **1996**, *118*, 8329. (b) Sasaki, T.; Watanabe, M. *J. Am. Chem. Soc.* **1998**, *120*, 4682.
(14) (a) Sasaki, T.; Ebina, Y.; Tanaka, T.; Harada, M.; Watanabe, M.; Decher, G. *Chem. Mater.* **2001**, *13*, 4661. (b) Wang, L. Z.; Omomo, Y.; Sakai, N.; Fukuda, K.; Nakai, I.; Ebina, Y.; Takada, K.; Watanabe, M.; Sasaki, T. *Chem. Mater.* **2003**, *15*, 2873. (c) Wang, L. Z.; Ebina, Y.; Takada, K.; Sasaki, T. *J. Phys. Chem. B* **2004**, *108*, 4283.

Substrates, including a quartz glass platelet and Si wafer chip (1×5 cm^2), were cleaned by treatment in a bath of methanol/HCl (1/1 in volume) and concentrated H_2SO_4 for 30 min each. The substrate was immersed in poly(diallyldimethylammonium) (PDDA) chloride solution (20 g dm^{-3}; pH 9.1) for 20 min to attain a positively charged surface, followed by washing with copious amounts of pure water. Then, the substrate was dipped in a colloidal suspension of nanosheets (0.08 g dm^{-3}; pH 9.1) for 20 min and washed again. A series of these operations was repeated n times to obtain multilayer films of $[PDDA/Ti_{(5.2-2x)/6}Mn_{x/2}O_2]_n$. The resulting film was dried under an N_2 gas stream.

Characterization. X-ray diffraction (XRD) patterns were collected using a Rigaku RINT-2000 powder diffractometer with graphite-monochromatized Cu Kα radiation ($\lambda = 0.15405$ nm). Lattice constants were refined by a least-squares procedure.[15] Crystal structures were also refined by Rietveld analysis procedure using the computer program RIETAN-2000.[16]

Metal content of titanates was analyzed by ICP spectrophotometer (SII NanoTechnology, SPS1700HVR) after dissolving a weighed sample amount with mixed acid of H_2SO_4 + HF. Raman measurements were performed in a backward microconfiguration, using the 514.5 nm line from an Ar^+ laser ($\sim$1 μW) focused to $\sim$2 μm diameter spot on the sample surface. The scattered light was dispersed by a subtractive triple spectrometer (HORIBA-Jobin Yvon T64000) and collected with a liquid-nitrogen-cooled charge-coupled device (CCD) detector. X-ray absorption near-edge structure (XANES) measurements were performed at the Photon Factory BL-12C in Institute of Materials Structure Science, High Energy Accelerator Research Organization (KEK-PF), Japan. Mn K-edge X-ray absorption fine structure (XAFS) spectra were recorded in the energy range from 6520 to 6600 eV for the XANES region.

Atomic force microscopy (SII NanoTechnology, E-Sweep) was used to observe a topographical image of the ultrathin films. Measurements were carried out in tapping mode using Si-tip cantilevers (force constant: 14 N·m^{-1}). UV−visible absorption spectra for the multilayer films fabricated on a quartz glass substrate were recorded in transmission mode using a Hitachi U-4000 spectrometer.

Magnetic susceptibilities were collected using a Quantum Design magnetic property measurement system. All magnetic data were corrected for the diamagnetism of the substrate and sample holder. Magnetic circular dichroism (MCD) measurements (200−900 nm) at 300 K were carried out using a UV−visible magneto-optical spectrometer (NEOARK BK800M) with Kerr configuration in a magnetic field normal to the substrate. Hard X-ray photoelectron spectroscopy (HX-PES) was performed at SPring-8 (BL15XU, $h\nu = 5.95$ keV at 300 K).[17] Binding energy was calibrated using the Fermi level of gold film.

First-Principles Calculation. First-principles calculation was performed to investigate electronic structures in $Ti_{1-x}Mn_xO_2$ nanosheets, and analyze the properties of these electronic structures related to ferromagnetism. The software package CASTEP was used in our calculation, which is based on a total-energy plane-wave method within a local spin-density approximation.[10,11]

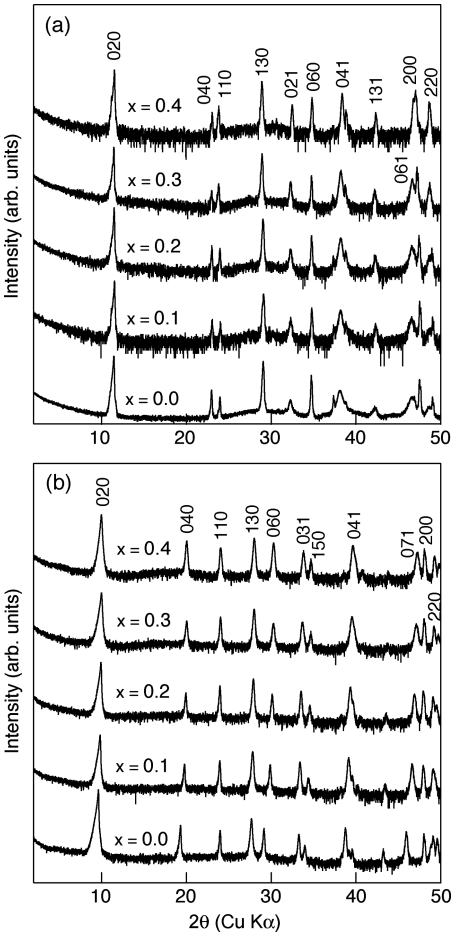

Figure 1. XRD patterns of Mn-substituted layered titanates $K_{0.8}Ti_{(5.2-2x)/3}Li_{(0.8-x)/3}Mn_xO_4$ ($x = 0.0, 0.1, 0.2, 0.3, 0.4$) (a) and their protonic materials $H_{(3.2-x)/3}Ti_{(5.2-2x)/3}Mn_xO_4 \cdot H_2O$ (x = 0.0, 0.1, 0.2, 0.3, 0.4) (b). XRD intensity is shown in log-scale.

Results and Discussion

Synthesis of Layered Materials. We employed Li-containing layered titanate as a starting material. Figure 1 shows the powder XRD data for the potassium lithium titanates $[K_{0.8}Ti_{(5.2-2x)/3}Li_{(0.8-x)/3}Mn_xO_4]$ and acid-exchanged titanates, for which the diffraction peaks can be indexed as a *C*-base-centered orthorhombic cell and body-centered orthorhombic cell, respectively. Refinement of unit cell dimensions (Table 1) also confirmed a layered structure of lepidocrocite type with orthorhombic cell, and agrees well with the nonsubstituted case.[12] A comparison between panels a and b in Figure 1 reveals that the layer structure is preserved with an interlayer expansion from 0.78−0.92 nm.

Rietveld refinement of the potassium lithium titanates $[K_{0.8}Ti_{(5.2-2x)/3}Li_{(0.8-x)/3}Mn_xO_4]$ was performed to characterize the accommodation sites of Li and Mn ions. The fitting results and final structure parameter for the heavily substituted case (x = 0.4) are shown in Supporting Information (Figure S1 and Table S1). The refinement

(15) Appleman, D. E.; Evans, H. T., Jr. *Report No. PB6188*; U.S. Department of Commerce, National Technical Information Service: Springfield, VA, 1973.
(16) (a) Izumi, F.; Ikeda, T. *Mater. Sci. Forum* **2000**, *321−324*, 198. (b) Izumi, F.; Dilanian, R. A. In *Recent Research Developments in Physics*; Transworld Research Network: Trivandrum, India, 2003; Vol. *3*, Part II, pp 699−726.
(17) (a) Kobayashi, K.; Yabashi, M.; Takata, Y.; Tokushima, T.; Shin, S.; Tamasaku, K.; Miwa, D.; Ishikawa, T.; Nohira, H.; Hattori, T.; Sugita, Y.; Nakatsuka, O.; Sakai, S.; Zaima, S. *Appl. Phys. Lett.* **2003**, *83*, 1005. (b) Takata, Y.; Yabashi, M.; Tamasaku, K.; Nishino, Y.; Miwa, D.; Ishikawa, T.; Ikenaga, E.; Horiba, K.; Shin, S.; Arita, M.; Shimada, K.; Namatame, H.; Taniguchi, M.; Nohira, H.; Hattori, T.; Sodergren, S.; Wannberg, B.; Kobayashi, K. *Nucl. Inst. Methods A*, **2005**, *547*, 50.

Table 1. Refined Lattice Parameters of Mn-Substituted Layered Titanates and Their Protonic Forms

sample	*a* (nm)	*b* (nm)	*c* (nm)
Mn-Substituted Layered Titanates $K_{0.8}Ti_{(5.2-2x)/3}Li_{(0.8-x)/3}Mn_xO_4$			
$x = 0.0$[a]	0.38237(2)	1.5532(1)	0.29727(3)
$x = 0.1$	0.38216(2)	1.5475(1)	0.29698(3)
$x = 0.2$	0.38322(3)	1.5479(1)	0.29691(3)
$x = 0.3$	0.38500(2)	1.5469(1)	0.29668(3)
$x = 0.4$	0.38597(3)	1.5438(1)	0.29530(1)
Protonic Form $H_{(3.2-x)/3}Ti_{(5.2-2x)/3}Mn_xO_4 \cdot H_2O$			
$x = 0.0$[a]	0.37852(2)	1.8402(2)	0.29962(3)
$x = 0.1$	0.37911(3)	1.7915(1)	0.29980(2)
$x = 0.2$	0.37905(2)	1.7780(2)	0.29899(2)
$x = 0.3$	0.37862(2)	1.7694(2)	0.29778(2)
$x = 0.4$	0.37803(3)	1.7685(2)	0.29680(3)

[a] The refined lattice parameters of nonsubstituted titanates are taken from ref 12.

confirms that both Li and Mn ions are incorporated into octahedral Ti sites in the host layers. Substitution of Li/Mn ions for Ti^{4+} ions in the nominal TiO_2 framework gives a negative charge that is balanced by interlayer K ions. Accommodation of Li ions in octahedral environments has been widely found in a variety of materials including lepidocrocite titanates $ATi_{2-x/3}Li_{x/3}O_4$ (A = K, Rb, and Cs),[12] spinels $Li_{1.33}Ti_{1.67}O_4$ and clay minerals (hectorite). In the Li/Mn-codoped case, we examined another possibility for Li location: Li ions in the interlayer space/vacancies at Ti sites. These models gave an unstable positional parameter and an unreasonable thermal factor for Li ions.

Raman spectra also supported the above structural model on Li/Mn sites (see the Supporting Information, Figure S2). Local structural features induced by Li/Mn cosubstitution are noticeable in the high-frequency region (600−1000 cm^{-1}). Raman modes at 600−1000 cm^{-1} stem from Ti−O bonds in TiO_6 octahedral host layers,[18] and thus spectral modification in this region are strongly correlated to the nature of the lattice dopants in the octahedral Ti sites. From these results as well as from a viewpoint of crystal chemistry, we conclude that both Li and Mn ions are situated in the octahedral site of the host framework.

Chemical analysis (Table 2) revealed that the Mn content was systematically changed by Li^+ doping in $K_{0.8}Ti_{(5.2-2x)/3}Li_{(0.8-x)/3}Mn_xO_4$, and the acid exchange did not bring about a significant change in Mn content. We also noted that almost all of the constituent alkali metal ions were extracted by acid leaching for 3 days, a situation similar to that of the nonsubstituted case

Table 2. Chemical Analysis Results of Mn-Substituted Layered Titanates and Their Protonic Materials[a]

sample		K	Li	Ti	Mn	Ig loss[b]
Mn-Substituted Layered Titanates $K_{0.8}Ti_{(5.2-2x)/3}Li_{(0.8-x)/3}Mn_xO_4$						
$K_{0.8}Ti_{1.73}Li_{0.27}O_4$	$x = 0.0$[c]	17.4	1.0	46.0	0	0
(calcd value)		(17.4)	(1.0)	(46.1)	(0)	(0)
$K_{0.8}Ti_{1.67}Li_{0.23}Mn_{0.1}O_4$	$x = 0.1$	17.4	0.9	43.6	3.0	0.8
		(17.2)	(0.9)	(43.9)	(3.0)	(0.4)
$K_{0.8}Ti_{1.6}Li_{0.2}Mn_{0.2}O_4$	$x = 0.2$	17.3	0.7	41.3	5.9	1.1
		(17.0)	(0.8)	(41.6)	(6.0)	(0.9)
$K_{0.8}Ti_{1.53}Li_{0.17}Mn_{0.3}O_4$	$x = 0.3$	17.0	0.6	39.1	8.7	1.1
		(16.8)	(0.6)	(39.4)	(8.9)	(1.3)
$K_{0.8}Ti_{1.47}Li_{0.13}Mn_{0.4}O_4$	$x = 0.4$	16.9	0.5	37.0	11.5	1.0
		(16.6)	(0.5)	(37.3)	(11.7)	(1.7)
Protonic Form $H_{(3.2-x)/3}Ti_{(5.2-2x)/3}Mn_xO_4 \cdot H_2O$						
$H_{1.07}Ti_{1.73}O_4 \cdot H_2O$	$x = 0.0$[c]	0	0	49.8	0	17.2
		(0)	(0)	(49.9)	(0)	(16.7)
$H_{1.03}Ti_{1.67}Mn_{0.1}O_4 \cdot H_2O$	$x = 0.1$	0	0	47.6	3.3	16.9
		(0)	(0)	(47.5)	(3.3)	(16.7)
$H_{1.0}Ti_{1.6}Mn_{0.2}O_4 \cdot H_2O$	$x = 0.2$	0	0	45.0	6.6	16.9
		(0)	(0)	(44.9)	(6.4)	(16.8)
$H_{0.97}Ti_{1.53}Mn_{0.3}O_4 \cdot H_2O$	$x = 0.3$	0	0	42.5	9.5	17.1
		(0)	(0)	(42.4)	(9.5)	(16.9)
$H_{0.93}Ti_{1.47}Mn_{0.4}O_4 \cdot H_2O$	$x = 0.4$	0	0	40.0	12.6	17.0
		(0)	(0)	(40.2)	(12.5)	(16.9)

[a] Values are in weight percent. [b] Weight loss at 1273 K. The O_2 release via reduction of Mn^{3+} to Mn^{2+} upon heating at 1273 K is taken into account for calculated Ig loss values. [c] Values from ref 12.

$[K_{0.8}(Ti_{1.73}Li_{0.27})O_4]$.[12] Mn *K*-edge XAFS spectra (see the Supporting Information, Figure S3) for the potassium lithium titanates $[K_{0.8}Ti_{(5.2-2x)/3}Li_{(0.8-x)/3}Mn_xO_4]$ and these acid-exchanged titanates showed a closer match to that of Mn_2O_3 (Mn^{3+}), showing that the Mn^{3+} oxidation state was preserved upon the acid exchange.[19] These structural and compositional changes upon acid exchange indicate that controlled Mn^{3+} doping was also achieved in protonic forms $H_{(3.2-x)/3}Ti_{(5.2-2x)/3}Mn_xO_4 \cdot H_2O$, where both the interlayer K^+ and intralayer Li^+ ions were completely extracted by acid-exchange reaction.

Preparation and Characterization of Nanosheets. The protonated samples $H_{(3.2-x)/3}Ti_{(5.2-2x)/3}Mn_xO_4 \cdot H_2O$ were reacted with aqueous solution containing TBA ions equivalent to the ion-exchanged protons in the solid. After intermittent shaking for 10 days, semitransparent colloidal suspensions were obtained. These suspensions exhibited clear Tyndall light scattering (Figure 2), demonstrating the presence of exfoliated nanosheets dispersed in the aqueous suspension.

XRD analysis of the colloids recovered by high-speed centrifugation provided further evidence of exfoliation reactions. Figure 3 shows XRD pattern for the colloidal aggregate of $Ti_{(5.2-2x)/6}Mn_{x/2}O_2$ ($x = 0.4$) nanosheets. Upon interaction with aqueous TBA ions, the pattern changed dramatically from that of the layered material to a broad profile. All sharp XRD peaks for the starting layered material disappeared. Similar phenomena have been observed in $Ti_{(5.2-2x)/6}Mn_{x/2}O_2$ with different x as well as other exfoliated nanosheets.[13b,20,21a,21b] The halo-like patterns were dependent on the layered materials and proved to be very similar to the square of the structure factor with the scattering vector normal to the sheet,

(18) (a) Gao, T.; Fjellvåg, H.; Norby, P. *J. Phys. Chem. B* **2008**, *112*, 9400. (b) Gao, T.; Fjellvåg, H.; Norby, P. *J. Mater. Chem. B* **2009**, *19*, 787.

(19) As has been demonstrated for various types of manganese oxides, the acid-exchanged treatment of manganese oxides often proceeds via two reaction routes: ion exchange and redox deintercalation involving disproportionation of $2Mn^{3+}(solid) \rightarrow Mn^{4+}(solid) + Mn^{2+}(solution)$. In our $K_{0.8}Ti_{(5.2-2x)/3}Li_{(0.8-x)/3}Mn_xO_4$ (x = 0.0−0.4) case, such a reaction indeed occurred by using of the dilute conditions (e.g., 0.1 mol dm^{-3}), where Mn ions were dissolved in acid solution and Mn content was reduced in the lattice. From these results, we choose the acid-exchanged treatment with 1 mol dm^{-3} HCl in this study.

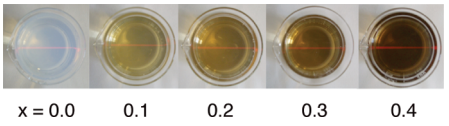

Figure 2. Photographs of colloidal suspensions of exfoliated $Ti_{(5.2-2x)/6}Mn_{x/2}O_2$ (x = 0.0, 0.1, 0.2, 0.3, 0.4) nanosheets. The light beam was incident from the side to demonstrate the Tyndall effect. Nanosheet concentration was 0.08 g dm^{-3}.

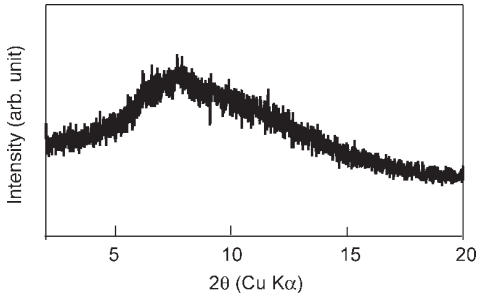

Figure 3. XRD pattern for the colloidal aggregate centrifuged from the suspension of $Ti_{(5.2-2x)/6}Mn_{x/2}O_2$ (x = 0.4) nanosheets.

indicating that the host layers were no longer parallel at a constant separation, which can be taken as evidence of total delamination.

AFM images of the nanosheet film displayed sheets showing sharp edges (Figure 4). The average thickness was 1.4 ± 0.1 nm, and the lateral size was several hundred nanometers. The thickness is consistent with that of the host layer deduced from the crystallographic data for nonsubstituted $Ti_{0.91}O_2$;[20] the vertical distance between the levels of upper and bottom oxygen atoms of the host layer (0.42 nm) plus the ionic radius of these two oxygen atoms (0.28 nm) gives 0.70 nm. This agreement further supports the unilamellar nature of the obtained nanosheet crystallites. The difference between the experimental height and crystallographic thickness may stem from adsorbed charge-compensating protons, oxonium ions, or water molecules, as is the case for other nanosheets.[20,21]

Self-Assembly of Multilayer Films. Fabrication of self-assembled multilayer films could be obtained by alternately dipping a quartz glass slide into PDDA solution and a colloidal suspension of the nanosheets. Figures 5 and 6 illustrate the buildup process of [PDDA/$Ti_{0.83}Mn_{0.05}O_2$ (x = 0.4)] multilayer films monitored by UV−visible absorption and XRD. The growth of [PDDA/$Ti_{(5.2-2x)/6}Mn_{x/2}O_2$] multilayer films under optimized conditions was demonstrated by UV−visible absorption

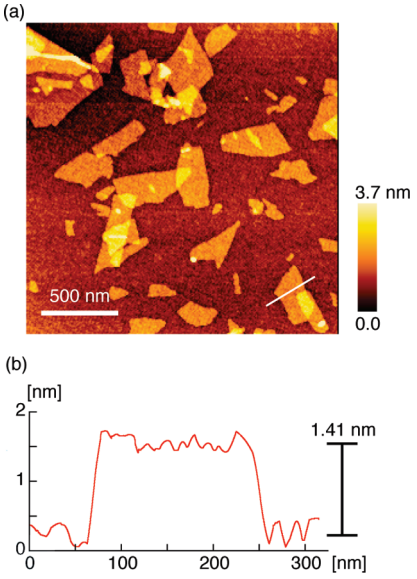

Figure 4. (a) Tapping-mode AFM image of exfoliated $Ti_{(5.2-2x)/6}Mn_{x/2}O_2$ (x = 0.4) nanosheets deposited on a Si wafer substrate. (b) Height profile of marked line in (a).

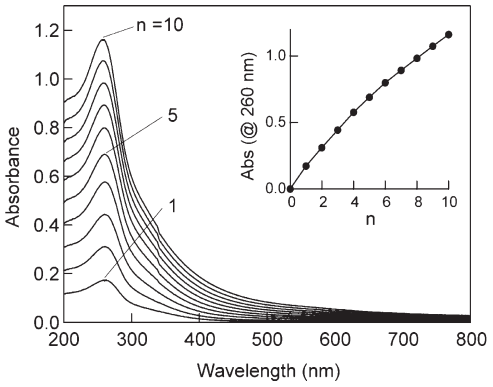

Figure 5. UV−visible absorption spectra for multilayer film of [PDDA/$Ti_{(5.2-2x)/6}Mn_{x/2}O_2]_n$ (n = 0 − 10) assembled on a quartz glass substrate. Nanosheet concentration was 0.08 g dm^{-3}; PDDA concentration was 20 g dm^{-3}; the pH value of PDDA solution and nanosheet suspension was 9; deposition time was 20 min. (Inset) Observed absorbance at 260 nm as a function of the deposition cycle, n.

spectra measured immediately after each deposition cycle (Figure 5). The absorption band around 260 nm is characteristic of titania nanosheets, and its nearly linear increment as a function of the number of deposition cycles indicates stepwise and regular film growth. After the deposition of 10 bilayers, absorbance at 260 nm was 1.3, which is comparable to that for the (PDDA/$Ti_{0.91}O_2)_{10}$ film.

XRD patterns (Figure 6) of the multilayer films illustrate the evolution of a Bragg peak at 6−7° in 2θ, which is attributable to a so-called superlattice reflection of the (PDDA/nanosheet)-repeating nanostructure.[14a] Periodicity of 1.2−1.4 nm was consistent with that observed for the (PDDA/$Ti_{0.91}O_2)_{10}$ film. Peak intensity increased progressively with the increase in the number of layer pairs, further verifying the successful multilayer buildup. Allowing for nanosheet thickness of about 0.7 nm, the layer height of PDDA along the film normal is estimated to be about 0.5−0.7 nm.

(20) (a) Sasaki, T.; Ebina, Y.; Kitami, Y.; Watanabe, M.; Oikawa, T. *J. Phys. Chem. B* **2001**, *105*, 6116. (b) Omomo, Y.; Sasaki, T.; Wang, L. Z.; Watanabe, M. *J. Am. Chem. Soc.* **2003**, *125*, 3568. (c) Fukuda, K.; Ebina, Y.; Shibata, T.; Aizawa, T.; Nakai, I.; Sasaki, T. *J. Am. Chem. Soc.* **2007**, *129*, 202. (d) Fukuda, K.; Nakai, I.; Ebina, Y.; Ma, R. Z.; Sasaki, T. *Inorg. Chem.* **2007**, *46*, 4787. (e) Ozawa, T. C.; Fukuda, K.; Akatsuka, K.; Ebina, Y.; Sasaki, T. *Chem. Mater.* **2007**, *19*, 6575.

(21) (a) Li, L.; Ma, R. Z.; Ebina, Y.; Iyi, N.; Sasaki, T. *Chem. Mater.* **2005**, *17*, 4386. (b) Liu, Z. P.; Ma, R. Z.; Osada, M.; Iyi, N.; Ebina, Y.; Takada, K.; Sasaki, T. *J. Am. Chem. Soc.* **2006**, *128*, 4872. (c) Ma, R. Z.; Liu, Z. P.; Li, L.; Iyi, N.; Sasaki, T. *J. Mater. Chem.* **2006**, *16*, 3809. (d) Ma, R. Z.; Liu, Z. P.; Takada, K.; Iyi, N.; Bando, Y.; Sasaki, T. *J. Am. Chem. Soc.* **2007**, *129*, 5257. (e) Ma, R. Z.; Takada, K.; Fukuda, K.; Iyi, N.; Bando, Y.; Sasaki, T. *Angew. Chem., Int. Ed.* **2008**, *47*, 86.

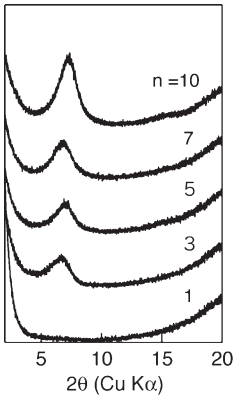

Figure 6. XRD patterns of multilayer films of $[PDDA/Ti_{(5.2-2x)/6}Mn_{x/2}O_2]_n$ ($x = 0.4$; $n = 1, 3, 5, 7, 10$) assembled on quartz glass substrates.

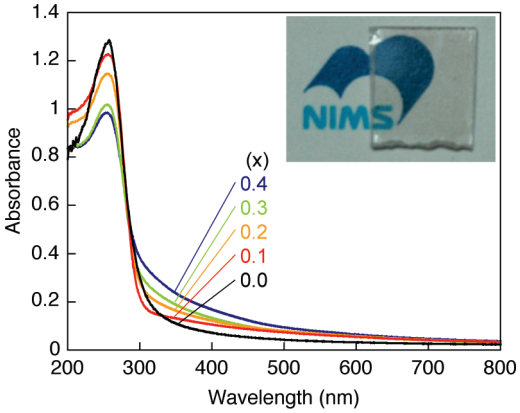

Figure 7. Comparison of UV−visible absorption spectra for multilayer films of $[PDDA/Ti_{(5.2-2x)/6}Mn_{x/2}O_2]_{10}$ ($x = 0.0, 0.1, 0.2, 0.3, 0.4$) assembled on quartz glass substrates. (Inset) Photograph of $[PDDA/Ti_{(5.2-2x)/6}Mn_{x/2}O_2]_{10}$ ($x = 0.4$) deposited on a quartz glass substrate.

Characterization of Multilayer Films. Figure 7 compares the absorption spectra for 10 layered films with different Mn content. Sharp interband absorption, characteristic of nanosheets,[14a] appears around 260 nm, and in-gap absorption increases with Mn substitution. Even up to such a high Mn content, the films of $Ti_{(5.2-2x)/6}Mn_{x/2}O_2$ were transparent in visible light, as is also illustrated in the inset of Figure 7. These optical properties, which are also observed in DMS,[4c] stem from the partially filled characteristic of 3d elements.

Hard X-ray photoelectron spectroscopy (HX-PES) at the Mn 2p core level was performed to determine the oxidation state and local geometry of the Mn dopant in the lattice. HX-PES has the significant advantage of bulk sensitivity due to the large probing depth of photoelectrons of several nanometers and therefore, provides a unique opportunity to investigate intrinsic electronic structures reflected on the entire volume of nm-thick films.[22] Figure 8 shows Mn 2p core-level spectra for 10 layered $[PDDA/Ti_{(5.2-2x)/6}Mn_{x/2}O_2]$ films with different Mn content. A main Mn $2p_{3/2}$ peak appears at 641.5 eV, accompanied by a satellite peak around 648 eV, with the

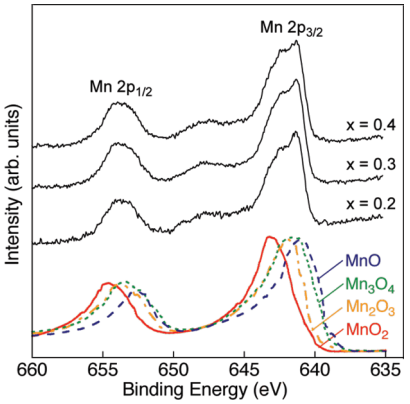

Figure 8. Mn 2p core-level spectra for $[PDDA/Ti_{(5.2-2x)/6}Mn_{x/2}O_2]_{10}$ ($x = 0.2, 0.3, 0.4$). For a comparison, data of the reference samples MnO (Mn^{2+}), Mn_3O_4 ($Mn^{2.66+}$), Mn_2O_3 (Mn^{3+}), and MnO_2 (Mn^{4+}) are also included.

Mn $2p_{1/2}$ peak appearing at 653.9 eV. The main Mn $2p_{3/2}$ peaks were not simple symmetric peaks, but instead exhibited complex line shapes arising from the mixed-valence state. A comparison with XPS spectra obtained from MnO_2 (+4), Mn_2O_3 (+3), Mn_3O_4 (+2.67), MnO (+2),[23] $Ti_{(5.2-2x)/6}Mn_{x/2}O_2$ spectra, together with the Mn $2p_{3/2}$ energy, shows a closer resemblance to Mn_3O_4 (+2.67). We therefore consider that $Ti_{(5.2-2x)/6}Mn_{x/2}O_2$ exhibits mixed-valence states with the coexistence of (Mn^{2+}/Mn^{3+}) ions. This reduction of oxidation state from Mn^{3+} in the starting formula is possibly taken place in the delamination process in basic media of TBAOH. We also noted that there is little variation in spectral line shape and peak binding energy of Mn 2p and Ti 2p core-level spectra with Mn content, showing that the local electronic structure of Mn impurities in $Ti_{(5.2-2x)/6}Mn_{x/2}O_2$ nanosheets is largely independent of x (see the Supporting Information, Figure S4). These results indicate that controlled (Mn^{2+}/Mn^{3+}) doping is achieved in exfoliated $Ti_{(5.2-2x)/6}Mn_{x/2}O_2$ ($x = 0.0-0.4$) nanosheets.

Such multilayer films constructed with 2D nanosheets are of intrinsic fundamental interest since magnetic properties in 2D systems are expected to be substantially different from those in 3D bulk systems. Indeed, we found that multilayer assemblies of Co, Fe-substituted titania nanosheets exhibited robust magneto-optical response at short wavelengths.[9,10] Since the present nanosheets exhibit mixed-valence states with the coexistence of (Mn^{2+}/Mn^{3+}) ions, a ferromagnetic property may be expected.

Figure 9 shows RT magnetization ($M-H$) of $Ti_{(5.2-2x)/6}Mn_{x/2}O_2$ nanosheets with different x composition. These films show a clear ferromagnetic hysteresis in similar to what observed in ferromagnetic $Ti_{1-x}Co_xO_2$ nanosheets.[9,10] The ferromagnetic state is stable up to $x = 0.4$, in which a maximum magnetic moment of ~0.67 μ_B/Mn is observed. To confirm the observed ferromagnetism in $Ti_{(5.2-2x)/6}Mn_{x/2}O_2$ nanosheets, we also investigated MCD spectroscopy, which is very useful for probing the

(22) Terai, K.; Yoshii, K.; Takeda, Y.; Fujimori, S. I.; Saitoh, Y.; Ohwada, K.; Inami, T.; Okane, T.; Arita, M.; Shimada, K.; Namatame, H.; Taniguchi, M.; Kobayashi, K.; Kobayashi, M.; Fujimori, A. *Phys. Rev. B* **2008**, *77*, 115128.

(23) (a) Oku, M.; Hirokawa, K. *J. Electron Spectrosc. Relat. Phenom.* **1976**, *8*, 475. (b) Moulder, J. F.; Stickle, W. F.; Sobol, P. E.; Bomben, K. D. *Handbook of X-ray Photoelectron Spectroscopy*; Perkin-Elmer Corp.: Eden Prairie, MN, 1992.

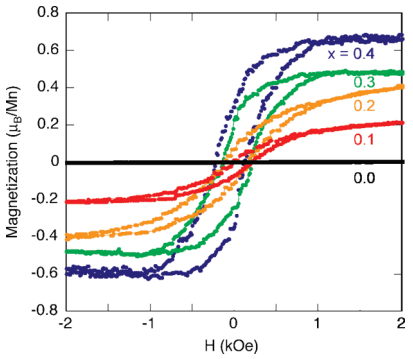

Figure 9. Magnetization curves for $[PDDA/Ti_{(5.2-2x)/6}Mn_{x/2}O_2]_{10}$ (x = 0.0, 0.1, 0.2, 0.3, 0.4) on a quartz glass substrate measured at RT with the field parallel to the film.

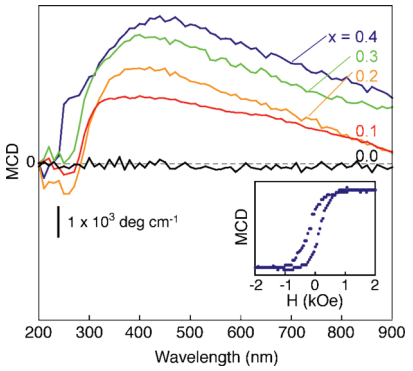

Figure 10. MCD spectra measured in 20 kOe at RT for $[PDDA/Ti_{(5.2-2x)/6}Mn_{x/2}O_2]_{10}$ (x = 0.0, 0.1, 0.2, 0.3, 0.4). Inset shows the magnetic field dependence of MCD for $[PDDA/Ti_{(5.2-2x)/6}Mn_{x/2}O_2]_{10}$ (x = 0.4) measured at 450 nm at RT.

magnetic properties of ultrathin films because the contribution from the substrate on the spectrum is negligible compared to the magnetization measurements.[24] Figure 10 shows RT MCD spectra of $Ti_{(5.2-2x)/6}Mn_{x/2}O_2$ nanosheets with different x composition. These films show a pronounced MCD response (2000−4500 deg cm^{-1}) around the absorption edge at 260−350 nm. This characteristic response thus reflects the Zeeman splitting induced by the O 2p−Mn 3d exchange interaction, a situation similar to that for $Ti_{0.8}Co_{0.2}O_2$ and $Ti_{0.6}Fe_{0.4}O_2$ nanosheets,[9,10] as well as DMS.[24,25]

In $Ti_{(5.2-2x)/6}Mn_{x/2}O_2$ nanosheets, the spectral features are quite different from those of $Ti_{0.8}Co_{0.2}O_2$ and $Ti_{0.6}Fe_{0.4}O_2$ nanosheets. Apart from sharp peaks near the absorption edge, $Ti_{(5.2-2x)/6}Mn_{x/2}O_2$ nanosheets exhibited some additional features extending from visible to near-infrared region. Broad features extending from 350 to 800 nm are analogous to d−d transitions (Co^{2+}−Fe^{3+}) in $Ti_{0.75}Fe_{0.1}Co_{0.15}O_2$. Therefore, the MCD features in $Ti_{(5.2-2x)/6}Mn_{x/2}O_2$ nanosheets are attributed to O 2p−Mn 3d and Mn d−d transitions. We also noted that these transitions are strongly dependent on Mn substitution. Figure 11 shows Mn-doping dependence of the MCD

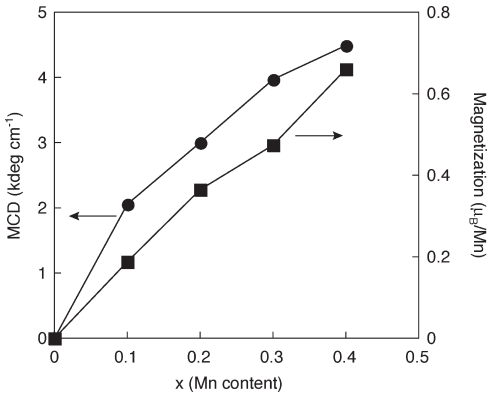

Figure 11. Mn-doping dependence of the MCD intensity at 450 nm and magnetic moment in $Ti_{(5.2-2x)/6}Mn_{x/2}O_2$ nanosheets.

intensity at 450 nm and magnetic moment in $Ti_{(5.2-2x)/6}Mn_{x/2}O_2$ nanosheets. Enhancement of magneto-optical properties is achieved by higher Mn substitution, a behavior resembles doping dependence of magnetization. The heavily doped $Ti_{(5.2-2x)/6}Mn_{x/2}O_2$ (x = 0.4) nanosheets exhibit large MO responses (~4500 deg cm^{-1}) over a wide wavelength region (350−800 nm). In addition, the magnetic field dependence of the MCD intensity at 450 nm (the inset of Figure 10) shows a clear ferromagnetic hysteresis, which coincides with the magnetization curve. The results were reproduced in films on different substrates and of different thicknesses. Also, the polymers used in the film assembly do not show any noticeable contribution in this spectral range. These characteristic responses thus reflect the intrinsic ferromagnetic behavior of $Ti_{(5.2-2x)/6}Mn_{x/2}O_2$ nanosheets.

To further investigate electronic structures, we performed a first-principles calculation on a monolayer Ti_3MnO_8 ($Ti_{0.75}Mn_{0.25}O_2$) cell. The calculated density of states (Figure 12a) indicates that the substituted Mn ions gives narrow bands in the forbidden gap, split due to the crystal field into t_{2g} and e_g states. These 3d states are hybridized with the O 2p band, which gives rise to strong magnetic coupling of two neighboring Mn ions mediated by O^{2-} ions. In such a case, d−d transitions are enabled or assisted through the overlapping of Mn 3d orbitals across the shared edges of adjacent octahedra and covalent bonding with oxygen. Such a band picture is consistent with HX-PES. In Figure 8, the presence of satellite structures indicates that the Mn 3d electronic state is influenced not only by strong Coulomb interaction between Mn 3d electrons but also by the hybridization between the Mn 3d orbitals and (ligand) O 2p bands. We also note that the calculated absorption spectrum (Figure 12b) yields pronounced d−d absorption bands in the in-gap visible range, which match the observed features in MCD spectra.

This situation is analogous to that in spinel oxides such as $MgMn_2O_4$,[26] where the d−d transitions take place between Mn^{3+} ions, mediated by O^{2-} ions. Indeed, the broad features at ~450 nm correspond well with the d−d transitions in $MgMn_2O_4$. Hence, we attribute the visible

(24) Ando, K. In *Magneto-optics of Diluted Magnetic Semiconductors: New Materials and Applications*; Sugano, S., Kojima, N., Eds.; Magnetio-Optics; Springer: Berlin, 2000; Chapter 7.
(25) Ando, K.; Saito, H.; Jin, Z.; Fukumura, T.; Kasawaki, M.; Matsumoto, Y.; Koinuma, H. *Appl. Phys. Lett.* **2001**, *78*, 2700.
(26) Bosi, F.; Hålenius, U.; Andreozzi, G. B.; Skogby, H.; Lucchesi, S. *Am. Mineral.* **2007**, *92*, 27.

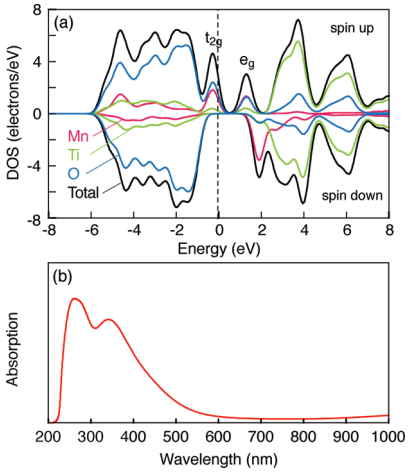

Figure 12. (a) Total and partial density of states (DOS) of monolayer Ti_3MnO_8 ($Ti_{0.75}Mn_{0.25}O_2$) cell. (b) Calculated optical absorption spectrum of the cell used in (a).

MO transitions in $Ti_{(5.2-2x)/6}Mn_{x/2}O_2$ nanosheets to the d−d transitions involving Mn^{3+}; the major transitions centered at 450 nm can be assigned to the d−d intervalence transitions of Mn^{3+}, whereas the weak features at 500−800 nm come from Mn d−d* transitions. We also noted that the strong magnetic coupling by Mn substitution seems to affect MCD intensity due to its correlation to the spin moments of the material.[24] Our nanosheets are composed entirely of surface atoms arranged two-dimensionally, and consequently, surface spins and their spin−orbit couplings are very strong, different from bulk materials.[9,10] This is a particular feature inherent to strong spin−orbit coupling, which yields a large MCD response from this material.

We also emphasize that our approach using $Ti_{(5.2-2x)/6}Mn_{x/2}O_2$ nanosheets promises to expand the range of possible material choices for future spintronic devices. In particular, such a large MCD response including the blue light region, together with the highly transparent characteristic, offers potential for short-wavelength magneto-optical applications. Current magneto-optical materials such as rare-earth iron garnet and $Cd_{1-x}Mn_xTe$ contain toxic elements, and thus are not environmentally benign.[27,28] In particular, $(Gd_{1-x}Bi_x)_3Fe_5O_{12}$ crystals often contain PbO flux because of technical difficulties in crystal growth, a current issue in the European RoHS (Restriction of Hazardous Substances) regulation. Thus, the use of environmentally benign magneto-optical materials is critically important to this field, and our approach with broad opportunities for creating additional magneto-optical activities provides a route to realize lead-free magneto-optical materials complying with the RoHS regulation.

(27) Booth, R. C.; White, E. A. D. *J. Phys. D: Appl. Phys.* **1984**, *17*, 579.
(28) Triboulet, R.; Didier, G. *J. Cryst. Growth* **1981**, *52*, 614.

Conclusion

We have succeeded in synthesizing $Ti_{(5.2-2x)/6}Mn_{x/2}O_2$ ($x = 0.0-0.4$) nanosheets by delaminating $[K_{0.8}Ti_{(5.2-2x)/3}Li_{(0.8-x)/3}Mn_xO_4]$, in which the Mn content was systematically controlled by Li^+ doping. Magnetic susceptibility and MCD measurements demonstrated that $Ti_{(5.2-2x)/6}Mn_{x/2}O_2$ nanosheets acted as nanoscale ferromagnetic layers at RT, and their multilayer assemblies exhibited large MO responses (~4500 deg cm^{-1}) over a wide wavelength region (350−800 nm). These results indicate that our approach using $Ti_{(5.2-2x)/6}Mn_{x/2}O_2$ nanosheets could potentially eliminate the previous problem of extrinsic impurities, while maintaining some concepts that have proven successful in low-dimensional DMS and superlattices. In particular, the capability of controlled doping in ferromagnetic nanomaterials is critically important to this field, and the solution-based assembly of ferromagnetic nanomaterials has great potential for the rational design and construction of complex nanodevices, even combined with transparent electronics and molecular devices. Although we have focused here only on magneto-optical properties, the assembled structure is naturally viewed as a tunnel junction, which could obviously be used in novel spin-electronic devices such as spin valves and optical interconnectors. In this context, the superlattice approach for ferromagnetic nanosheets is an important step toward practicability of these ideas.

Acknowledgment. This work was partly supported by a Grant-in-Aid for Construction of the World Premier Research Institute from the Ministry of Education, Culture, Sports, Science and Technology (MEXT), Japan and the Industrial Technology Research Grant Program (06A22702d), NEDO, Japan. The XANES measurements were carried out at the Photon Factory (Proposal No. 2009PF-01). The authors gratefully thank Dr. K. Fukuda (Shinshu University) for his assistance with XANES analysis. The HX-PES measurements were performed under the approval of NIMS Beamline Station (Proposals 2007A4608, 2007B4605, 2008A4602, and 2008A4800). The authors are grateful to HiSOR, Hiroshima University, and JAEA/SPring-8 for the development of HX-PES at BL15XU of SPring-8.

Supporting Information Available: Additional figures and information (PDF). This material is available free of charge via the Internet at http://pubs.acs.org.